

Thickness effect and double phase transitions in Ge₅₀Te₅₀ thin films prepared by PLD

S. HUSSEIN, H. GHAMLOUCHE*

Department of Physics and Electronics, Faculty of Sciences I, Lebanese University, Hadat, Lebanon

The phase change material binary compound Ge₅₀Te₅₀ thin films were prepared by Pulsed Laser Deposition technique (PLD). The effect of deposition time on the physical properties of the films has been investigated. The phase transition, the electrical measurements showed two phase transitions at different temperatures. The first is the standard transition from amorphous to crystalline phase, while the second is the transition in the crystalline state from rhombohedral to cubic phase. XRD and DSC measurements have been performed to confirm the existence of these two peaks.

(Received October 11, 2021; accepted August 10, 2022)

Keywords: Phase change materials, PLD, Ge₅₀Te₅₀, Double phase transitions

1. Introduction

Phase Change Materials (PCM) are rare class of compounds, which can be rapidly cycled between two or more states having different atomic arrangements, typically an amorphous and one or more crystalline phases. These states have largely different macroscopic properties, such as optical reflectivity, electronic resistivity, mass density, and thermal conductivity. Thus, the ability switching between these states paves the way for applications in information storage. As examples, the change in optical reflectivity is commonly employed in rewritable optical discs, while the contrast in electronic resistivity is utilized to develop resistive random access memory devices (PCRAM). While many other materials exhibit such two phases, the unique feature that classifies phase change materials is the combination of high structural stability of the two phases with very fast transitions between the two states (memory switching) [1-6].

From the many available phase change materials, the binary compound Ge₅₀Te₅₀ is among the most attractive ones owing to its good thermal stability material, significantly high crystallization velocity, and capacity of data retention at high temperatures. As a consequence, the growth of Ge₅₀Te₅₀ thin films has been investigated by several research groups, using a variety of materials synthesis techniques such as Evaporation, Sputtering, Atomic Layer Deposition. Recently, Javier *et al.* [7] prepared polycrystalline GeTe by using arc-melting and investigated the structural transition from rhombohedral to cubic by Differential Scanning Calorimetry (DSC) measurements. They found an endothermic peak at 425°C during the heating cycle corresponding to the structural phase transition, whereas an exothermic peak at 410°C is observed while cooling, thereby indicating a hysteretic effect related to a first-order transition. Another attractive physical deposition method, pulsed laser deposition (PLD) provides several characteristics including high quality

films, options for multi-compositions, quick and accurate control of the deposition process, a simple experimental set up, and the possibility of scaling up the process. However, only a few studies dealing with the preparation of phase-change films by PLD technique have been published. Xinxing Sun *et al.* [8] deposited GeTe films on Si substrates at room temperature by Pulsed Laser Deposition (PLD) and a significant resistivity drop (3–4 orders of magnitude) at a transition temperature ranging from 220 to 255°C. This effect was found to be correlated to the amorphous to crystalline (rhombohedral) phase transition and weakly dependent on the heating rate. In this paper, we report on the PLD of Ge₅₀Te₅₀ (GeTe) films with particular focus on the detection of phase transitions using X-Ray Diffraction, temperature dependent electrical resistance measurements as well as Differential Scanning Calorimetry (DSC).

2. Experimental

Thin films of GeTe were grown by PLD on glass, using a KrF excimer laser (CompexPro 205F, Coherent), emitting at a wavelength of 248 nm. The pulse energy and the pulse repetition rate were set to 200 mJ and 10 Hz respectively. The distance between the substrate and the commercially available Ge₅₀Te₅₀ (Testbourne Ltd.) target was fixed at 6 cm. In order to ensure homogeneous consumption of the target, the latter is mounted on rotary drives that allow rotation and toggling. Further technical details on the PLD system can be found elsewhere [9]. All films were deposited on ultrasonically degreased glass substrates at room temperature under a pure argon atmosphere at a pressure of 10⁻⁴ mbar.

XRD measurements were performed using a fully automated D8 Advance diffractometer from Bruker AXS systems. Imaging of the films' surface topography was also performed using a MIRA 3 series scanning electron microscope (SEM) equipped with a Schottky field emission

electron gun. An energy-dispersive X-ray spectroscopy (EDX) attachment to the SEM was utilized to get the films' composition. A Dektak XT surface Profilometer was used to measure the thicknesses of the films. Electrical properties were determined through measurements of the resistance of the films as a function of temperature using in-plane four collinear probes. Samples were thus cut into rectangular pieces ($10 \times 20 \text{ mm}^2$), and pasted using silver paint on a heated block whose temperature is measured using a thermocouple. Finally, a TA Instruments T2000 was used for the Differential Scanning Calorimetry (DSC) measurements.

3. Results and discussions

3.1. Effect of deposition time on the physical properties of $\text{Ge}_{50}\text{Te}_{50}$ thin films

In order to study the effect of varying the deposition time on the properties of the deposited GeTe films, five

samples were prepared at room temperature under the best conditions mentioned above but with different deposition times (1:30 h, 2 h, 2:30 h, 3 h and 3:30 h). These samples were characterized by different techniques and the corresponding results are presented below.

From the XRD measurements one can observe that all the as-grown five samples are in the amorphous phase, as shown in Fig. 1. The XRD patterns of all the deposited films show a very broad peak in the 2θ ranged between 25° and 30° , indicating an amorphous phase of all the five films.

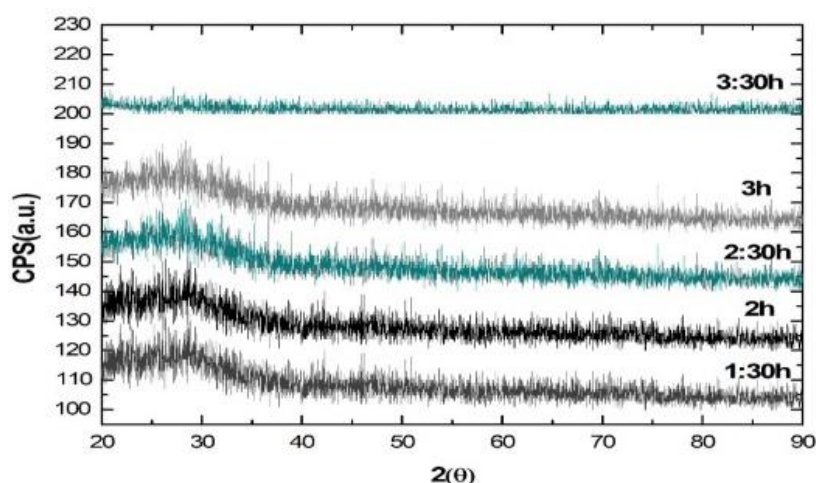


Fig. 1. XRD pattern of amorphous $\text{Ge}_{50}\text{Te}_{50}$ films deposited at different deposition time

Table 1 shows the thicknesses and compositions of the films determined by the Profilometer and EDX techniques. The film thickness increased from 293 nm to 418 nm as the deposition time increases from 1:30 h to 3:30 h. The deposition time has a strong influence on the film's thickness, as expected.

Table 1. Atomic composition and thickness of films deposited at different deposition time

Deposition time (hours)	Atomic Ge%	Atomic Te%	Thickness (nm)
1:30	53.89	46.17	293
2	52.97	47.03	321
2:30	52.40	47.60	351
3	51.16	48.84	385
3:30	53.73	46.27	418

As the deposition time increases, more elements in the target surface are heated up to their evaporation temperature

and thus more materials are dissociated from the target and ablated out. Therefore, as we increase the deposition time, more materials are removed from the target and deposited on the substrate, i.e. the thickness of the films increases.

It is noticed from Table 1 that the best film composition is obtained at a deposition time of 3 h. A further increase in the deposition time (3:30 h) introduces a deviation from stoichiometry (1.61%). The atomic percentage of Ge increases while that of Te decreases. This deviation from stoichiometry upon increasing the film thickness was previously reported in thin films [10-12].

The resistance measurements were carried out on the samples deposited at different deposition times as a function of temperature ($25^\circ\text{C} - 270^\circ\text{C}$) at a heating rate of $5^\circ\text{C}/\text{min}$. The resistance versus temperature curves are plotted to determine the amorphous-crystalline transition temperatures (T_c) and its width. These plots are shown in Fig. 2 for the five films deposited at different deposition times.

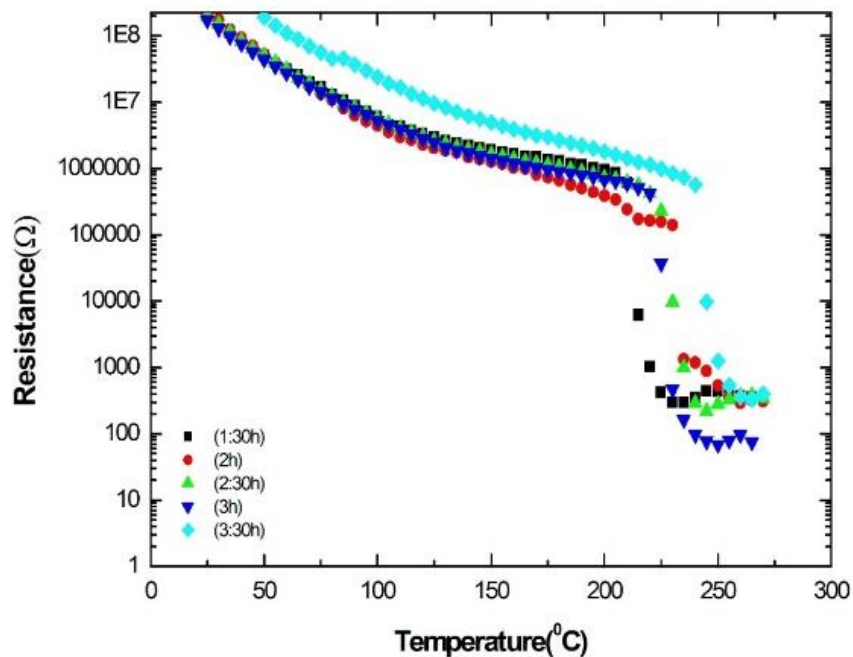


Fig. 2. Resistance as a function of temperature of the GeTe films deposited at different deposition times

As the temperature is raised from 25°C and on, the resistance starts decreasing. As the temperature reaches certain value, the resistance drops drastically by 3 orders of magnitude over a very narrow range. This resistance drop is related to the amorphous to crystalline phase transition. This increase in the conductivity upon transition is mainly

due to the increase of mobility, rather than of carrier concentration [13, 14]. By plotting $\ln(R)$ as a function of $1000/T$ (Arrhenius plot), the electrical bandgaps can be determined from the slopes of the curves of Fig. 3. The results are summarized in Table 2.

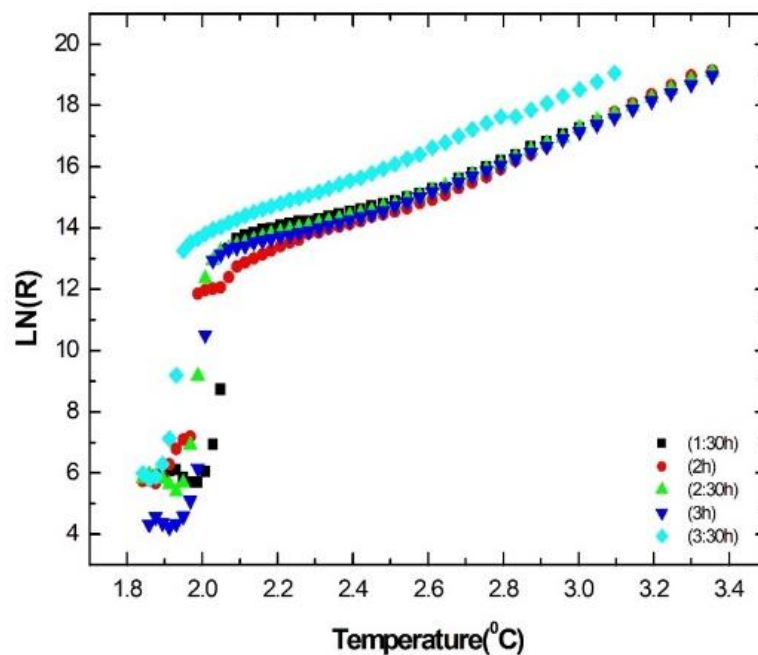


Fig. 3. Arrhenius Plots of $\ln(R)$ versus $1000/T$ for $Ge_{50}Te_{50}$ Films Deposited at Different deposition time

Table 2. Crystallization temperature (T_c), Electrical energy gap (E_g) and Transition width of the films deposited at different deposition times

Sample name	Deposition time	Energy gap E_g (eV)	T_c (°C)	Transition width (°C)
G7	1:30	0.74	212	15
G8	2	0.86	230	10
G9	2:30	0.75	227	15
G10	3	0.76	225	20
G12	3:30	0.81	242	15

Our results show relatively high transition temperatures in comparison to what have been reported previously [15]. Lower transition temperatures [180-200°C] have been reported however in most published works [16]. This difference in the transition temperatures values could be due to: the preparation technique, the quality of the film, stoichiometry of the material, and the level of disorder of atoms in the amorphous state etc... In what concerns the transition width, our values are very similar to what have been reported in literature [15, 16]. Our results show no significant effect of thickness (or a clear trend) on the energy gaps, transition temperatures and transition widths. The difference in values falls within the experimental errors (~5 %).

3.2. Observation of double phase transitions

3.2.1. Electric measurements

To investigate the multi-transitions observed in the resistance versus temperature curves of GeTe thin films, we have prepared samples under the best conditions mentioned before [9] and repeated here: laser energy (200 mJ), chamber pressure (10^{-4} mbar), frequency (10 Hz), substrate-target distance (6 cm), and for two deposition times (3 and 6 hours).

Resistance versus temperature and XRD measurements were carried out on four samples (two deposited for 3 hours and two for 6 hours). The resistance versus temperature measurement were done on S1 and S2 by heating from 25°C up to first transition temperature, which was about 190°C for S1 and 160°C for S2 and then stopped after the transition occurred by a few degrees; this process has been performed in order to do XRD measurements before the occurrence of the second transition above 250°C. Two other samples (S3 and S4) from the same batch of S1 and S2 were used to measure the resistance by heating now from 25°C up to the second transition temperature around 325°C. Fig. 4 shows the resistance versus temperature curves of S3 and S4 since they cover the whole range of temperatures.

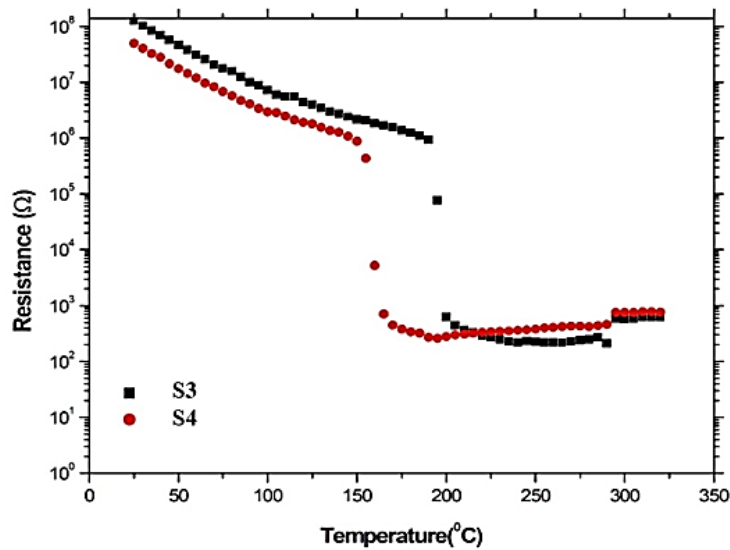


Fig. 4. Resistance versus temperature of samples S3 and S4 measured with a heating rate of 5°C/min

In order to find the electrical energy gap, we plotted $\ln(R)$ as a function of the reciprocal temperature (Arrhenius plot), as shown in Fig. 5. The results of the

electrical measurements on the samples are summarized in Table 3.

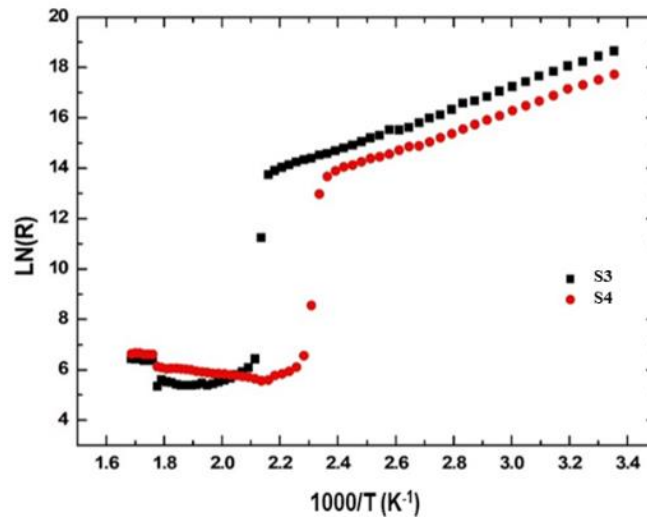


Fig. 5. Arrhenius plots of $\ln(R)$ versus $1000/T$ for samples S3 and S4

Table 3. The crystallization temperature (T_c), (Electrical band gap (E_g), and transition width of films deposited at different deposition time

Deposition time	E_g (eV)	T_c (°C)	Transition width (°C)
S3	0.70	190	20
S4	0.69	160	20

3.2.2. XRD measurements

Now in order to identify the phases before and after each transition, XRD measurements have been performed on the samples mentioned above, as shown in Fig. 6.

The XRD patterns were investigated to determine the crystallization behaviors of the $\text{Ge}_{50}\text{Te}_{50}$ films. Fig. 6 shows the XRD pattern of $\text{Ge}_{50}\text{Te}_{50}$ films at different heating temperatures. Due to the nature of the amorphous state there

is no obvious peak for the as-deposited film. The crystalline peaks started to appear after heating the films to the first transition temperatures. The plane indices of these peaks are given above the XRD pattern in Fig. 6. The results consistently show that $\text{Ge}_{50}\text{Te}_{50}$ films transform from amorphous to metastable rhombohedral phase at 190°C. When the temperature is higher than 300°C new peaks of the cubic phase appeared.

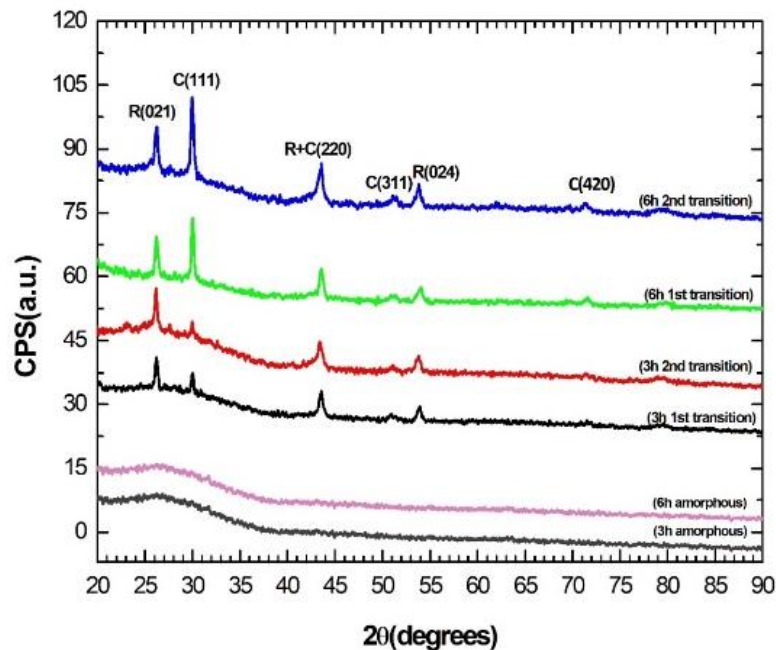


Fig. 6. XRD spectra of the as deposited films as well as of the films heated up to the first transition (3h-sample and 6-h sample) and up to the second transition (3h-sample and 6-h sample)

In order to further investigate the crystal structure at high temperatures, we annealed the amorphous samples at different temperatures (250, 300, 350, 380, 400 and 450) °C in vacuum oven for (15 min) then the samples were cooled down to room temperature before characterized them by XRD technique. The typical XRD patterns of Ge₅₀Te₅₀ films at rhombohedral and fcc states are shown in Fig. 7. The structural information is given by the peak positions and its relative intensity. The film annealed at 250°C is crystallized into a rhombohedral state indicated by XRD peaks (003), (021), (202), (220) and (042) [17]. Further

annealing at temperatures above 350°C leads to the transition from rhombohedral structure to the fcc closest packed (fcc) state shown by the XRD peaks (111), (220) and (222) [18-22].

We conclude that a phase change from a rhombohedral to a cubic structure occurs at around 350 °C. This is due to the fact that during the annealing process the atoms tend to move to the most active sites to lower their surface energy, under the thermal excitation. Therefore, more ordered crystallization can be obtained through annealing process [23, 24].

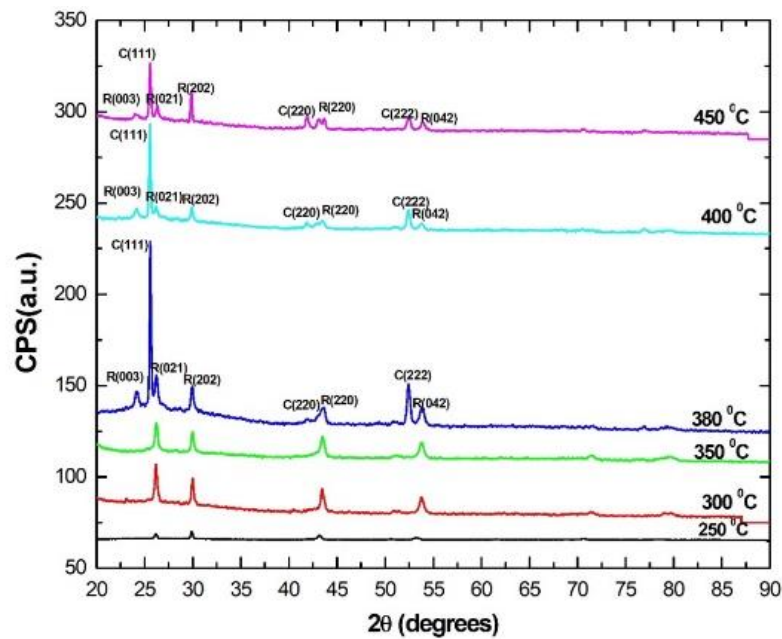


Fig. 7. XRD measurement of annealed samples at 250°C, 300°C, 350°C, 380°C, 400°C and 450°C

3.2.3. Differential Scanning Calorimetry (DSC)

Fig. 8 shows the DSC curves of Ge₅₀Te₅₀ target and many films with different masses: 0.4, 2.45, 3.09 and 4.28 mg. The temperature has been swept from 25°C up to 400°C under a heating rate of 10°C/min. From this figure we reveal

exothermic peak upon heating between 255°C and 280°C. This peak is associated with the phase transition from the amorphous phase to the rhombohedral phase [25]. The usual observations are that: the higher is the mass, the larger is the width and the larger is the maximum heat flow-rate, as seen in Fig. 8 [26, 27].

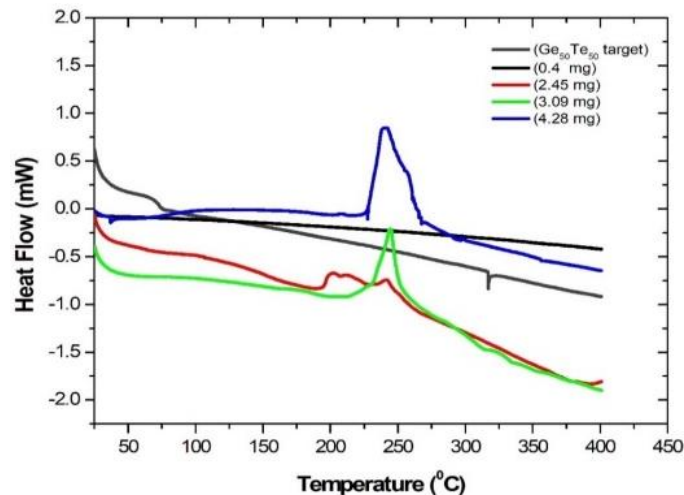


Fig. 8. DSC curves of Ge₅₀Te₅₀ for the target and for some films of various masses at a heating rate of 10 °C/min

In Fig. 9, we measured the heat flow of $\text{Ge}_{50}\text{Te}_{50}$ films of masses 2.92 and 5.47 mg under a heating rate of $5^\circ\text{C}/\text{min}$. This figure shows two peaks; the first one (at 238.72°C) is related to the phase transition from the amorphous to the rhombohedral phases, while the second peak (at 265.63°C) is related to the transition in the crystal state from the rhombohedral phase to the cubic phase. This confirms our observations in the electrical and the XRD measurements discussed above. Note that the second peak is much smaller than what has been mentioned in literature (426°C) [27].

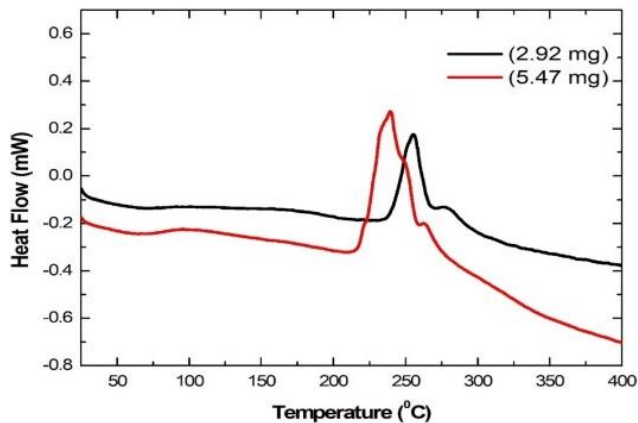


Fig. 9. DSC curves of $\text{Ge}_{50}\text{Te}_{50}$ for samples of mass of 2.92 and 5.47 mg at a heating rate of $5^\circ\text{C}/\text{min}$

We should mention, at the end, that the second peak has not been observed for a heating rate of $10^\circ\text{C}/\text{min}$. This could be explained as follows. The thermal gradient in the crucible is created as the constant heating rate is supplied, and the effect increases with increasing the heating rate or the sample size. This thermal gradient effect is very strong for PCMs in particular, since PCMs have a high thermal energy storage combined with a low thermal conductivity and heat diffusivity [28]. As a consequence, a gradient of temperature is developed throughout the material and the temperature is not uniform throughout the sample. The measured temperature by the DSC sensor, which is in direct contact with the specimen surface, is higher than the average sample temperature - especially at higher heating rate and sample mass. In this situation, a thermal lag exists between the thermocouples and the sample, and the instrument response becomes slow. Since the temperature difference between the average sample temperature and DSC sensor is due to the time necessary for the heat flux to dissipate through the sample, lower heating rates and sample masses, up to a certain limit, can help to reduce these effects. Therefore, lower heating rates and sample masses can help to reduce the thermal gradient effect and help to distinguish two separate transition peaks in some cases.

4. Conclusion

The phase change material binary compound $\text{Ge}_{50}\text{Te}_{50}$ thin films have been prepared by Pulsed Laser Deposition technique (PLD). Different parameters have been changed

in order to obtain very good quality amorphous thin films. The following preparation conditions have been used in order to get such good films: substrate-target distance of 6 cm, chamber atmosphere of 10^{-4} mbar, laser energy of 200 mJ and frequency of 10 Hz. Effects of deposition time (consequently the thickness) on the physical properties of the films have been investigated. The results show that the best film compositions were obtained at a deposition time of 3 h. No significant effect on the transition temperature, transition width nor on the energy gap values has been found. The slight change in the values might be attributed to the experimental errors (5-10%). In what concerns phase transitions, the electrical measurements showed two transitions at two different temperatures. The first is the standard transition from amorphous to crystalline phase, while the second is the transition in the crystalline state from rhombohedral to cubic phase. XRD and DSC measurements have been performed to confirm the existence of these two peaks. The XRD measurements were performed at different annealing temperatures, while the DSC measurements were conducted on the prepared films (amorphous) using different masses and heating rates. For the heating rate of 10°C , in the DSC measurements, only one big peak was observed. This peak represents the transition from amorphous phase to crystalline one. However, by using a heating rate of 5°C , an additional small peak at 255°C ($m = 2.99$ mg) and 280°C ($m = 5.47$ mg) was observed. The small peak might represent the phase transition between rhombohedral phase and cubic phase in the crystalline state.

Acknowledgements

The authors would like to thank the Lebanese University for the support of this project. The authors would like to acknowledge the Central Research Science Laboratory (CRSL) of AUB.

References

- [1] S. Kumar, V. Sharma, J. Alloys and Compounds **893**, 162316 (2022).
- [2] A. El-Denglawey, V. Sharma, E. Sharma, K. A. Aly, A. Dahshan, P. Sharma, J. Physics and Chemistry of Solids **159**, 110291 (2021).
- [3] K. Singh, S. Kumari, H. Singh, N. Bala, P. Singh, A. Kumar, A. Thakur, Accepted for publication, Appl Nanosci, (2021).
- [4] H. Singh, P. Singh, R. Singh, J. Sharma, A. P. Singh, A. Kumar, A. Thakur, Heliyon **5**, e02933 (2019).
- [5] P. Singh, A. P. Singh, J. Sharma, A. Kumar, M. Mishra, G. Gupta, A. Thakur, Phys. Rev. Appl. **10**, 054070 (2018).
- [6] P. Singh, A. P. Singh, N. Kanda, M. Mishra, G. Gupta, A. Thakur, Appl. Phys. Lett. **111**, 261102 (2017).
- [7] J. Gainza, F. S. Sánchez, N. M. Nemes,

- J. L. Martínez, M. T. F. Díaz, J. A. Alonso, *Metals* **10**, 48 (2020).
- [8] X. Sun, E. Thelander, J. W. Gerlach, U. Decker, B. Rauschenbach, *J. Phys. D: Appl. Phys.* **48**, 295304 (2015).
- [9] H. Ghamlouche, N. Choueib, M. Tabbal, R. Sayed Hassan, M. Hassan, *Applied Physics A* **124**, 200 (2018).
- [10] J. Jeong, *Advances in Materials Science and Engineering*, **2015**(5), 350196 (2015).
- [11] M. K. Baig, S. Atiq, S. Bashir, S. Riaz, S. Naseem, H. Soleimani, N. Yahya, *Journal of applied research and technology* **14**(5), 287 (2016).
- [12] P. Němec, M. Frumar, J. Jedelský, M. Jelinek, J. Lančok, I. Gregora, *Journal of Non-Crystalline Solids* **299**, 1013 (2002).
- [13] D. B. Chrisey, G. K. Hubler, *Pulsed laser deposition of thin films*, Wiley (1994).
- [14] K. Song, S. Beak, H. Lee, *Journal of Applied Physics* **108**(2), 024506 (2010).
- [15] J. H. Jeong, H. K. Kim, D. J. Choi, *J. Mater. Sci.* **48**, 6167 (2013).
- [16] E. Gourvest, S. Lhostis, J. Kreisel, M. Armand, S. Maitrejean, A. Roule, C. Vallée, *Appl. Phys. Lett.* **95**, 031908 (2009).
- [17] B. G. Sangeetha, M. R. Rahman, A. Akash, S. Govind, K. S. Santosh, S. Sumana, K. Suresh **2**(4-5), 1435 (2015).
- [18] X. Zhou, W. Dong, H. Zhang, R. E. Simpson, *J. Appl. Phys.* **107**, 074308 (2010).
- [19] J. Li, X. Zhang, Z. Chen, S. Lin, W. Li, J. Shen, I. T. Witting, A. Faghaninia, Y. Chen, A. Jain, L. Chen, G. J. Snyder, Y. Pei, *Joule* **2**(5), 976 (2018).
- [20] Q. Li, K. Xu, X. Wang, H. Huang, L. Ma, C. Bi, Z. Yang, Y. Li, Y. Zhao, S. Fan, J. Liua, C. Hu, *J. Mater. Chem. C* **7**, 4132 (2019).
- [21] Y. Yin, H. Zhang, S. Hosaka, Y. Liu, Q. Yu, *J. Phys. D: Appl. Phys.* **46**, 505311 (2013).
- [22] Z. Zhang, C. Peng, S. Song, Z. Song, Y. Cheng, K. Ren, X. Li, F. Rao, B. Liu, S. Feng, *J. Appl. Phys.* **114**, 244311 (2013).
- [23] E-S. Park, C. Yoo, W. Kim, M. Ha, J. W. Jeon, Y. K. Lee, C. S. Hwang, *Chem. Mater.* **31**, 8663 (2019).
- [24] A. A. El-Sebaili, S. Khan, F. M. Al Marzouki, A. S. Faidah, *Journal of Luminescence* **132**, 2082 (2012).
- [25] I. Krupa, G. Mikova, A. S. Luyt, *European Polymer Journal* **43**, 4695 (2007).
- [26] D. Kashchiev, *Nucleation: Basic Theory with Application*, Oxford: Butterworth-Heinemann, 2000.
- [27] G. W. H. Höhne, W. F. Hemminger, H.-J. Flammersheim, *Differential Scanning Calorimetry*, Springer Berlin Heidelberg New York, Chapter 6.3, 168 (2003).
- [28] H. Mehling, L. F. Cabeza, *Heat and cold storage with PCM*, Springer (2008).

* Corresponding author: hassan.ghamlouche@ul.edu.lb